PHYSICAL REVIEW B **92**, 060502(R) (2015)

Observation of a Raman-active phonon with Fano line shape in the quasi-one-dimensional superconductor $K_2Cr_3As_3$

W.-L. Zhang,[1,*] H. Li,[1] Dai Xia,[1] H. W. Liu,[1] Y.-G. Shi,[1] J. L. Luo,[1,2] Jiangping Hu,[1,2,3] P. Richard,[1,2,†] and H. Ding[1,2]

[1]*Beijing National Laboratory for Condensed Matter Physics and Institute of Physics, Chinese Academy of Sciences, Beijing 100190, China*

[2]*Collaborative Innovation Center of Quantum Matter, Beijing, China*

[3]*Department of Physics, Purdue University, West Lafayette, Indiana 47907, USA*

(Received 3 June 2015; published 13 August 2015)

We performed a polarized Raman scattering study of the quasi-one-dimensional superconductor $K_2Cr_3As_3$. We detect two A_1' phonons and three E' phonons. One of the A_1' modes exhibits a nearly temperature-independent Fano line shape. Based on our first-principles calculations, we ascribe this mode to the in-phase vibrations of Cr atoms within one layer. This observation suggests that the magnetic fluctuations in $K_2Cr_3As_3$ are coupled to the electronic structure via the lattice.

DOI: 10.1103/PhysRevB.92.060502 PACS number(s): 74.25.Kc, 63.20.kd, 74.25.nd, 79.60.−i

Superconductivity in conventional superconductors is mediated by the electron-phonon interaction. The electron-phonon coupling can manifest itself in the Raman response by an asymmetric profile of the spectral line shape of Raman phonons called the Fano line shape [1]. Despite a superconducting transition temperature (T_c) up to 6.1 K comparable to that of conventional superconductors, the recently discovered quasi-one-dimensional superconductors $A_2Cr_3As_3$ (A = K, Rb, Cs) have exotic properties that tentatively earned them the label of unconventional superconductors [2–4], such as an abnormal power law divergence of the ^{75}As nuclear spin lattice relaxation rate near T_c [5]. Penetration depth measurements suggest a nodal line in the superconducting gap [6], and a large zero temperature upper critical field $H_{c2}(0)$ compared to the Pauli limit has been attributed to a spin triplet p-wave pairing [2], in agreement with a theoretical study revealing strong ferromagnetic fluctuations caused by the frustration of Cr moments within one layer [7]. Interestingly, CrAs itself exhibits superconductivity, albeit under external pressure, in proximity to a magnetic instability [8]. Moreover, theoretical calculations of the electronic density of states indicate a sizable renormalization factor in $K_2Cr_3As_3$ compatible with a large specific heat coefficient [2], suggesting significant electronic correlations [9,10]. However, although some evidence pushes towards unconventional superconductivity in $K_2Cr_3As_3$, this view is not universally accepted [11] and whether the electron-phonon interaction plays a key role in this material remains an open question.

In this Rapid Communication, we report a polarized Raman scattering study of $K_2Cr_3As_3$. The symmetry of the vibration modes determined from our polarization study allows us to identify which atoms move and how they move. We observe two and three phonon modes with A_1' and E' symmetries, respectively. Surprisingly, one of the A_1' phonons exhibits a Fano line shape, nearly temperature independent from 12 K to room temperature, which is characterized by an electron-phonon coupling strength factor $1/q = -0.29$. Our theoretical analysis indicates that this mode involves the in-plane movement of the Cr atoms, which directly modulates the Cr-Cr bonding identified to be critical to the magnetic fluctuations in this system. Although our results are not sufficient to rule out a direct electron-phonon coupling in $K_2Cr_3As_3$, or to make a conclusive statement about the origin of superconductivity in this material, our results are suggestive of a lattice-mediated coupling between electrons and magnetic fluctuations.

The $K_2Cr_3As_3$ single crystals used in this Raman study have been synthesized by a self-flux method [2]. The needlelike samples have a typical size of $0.1 \times 0.1 \times 3$ mm^3. The crystal structure belongs to the space group $P\bar{6}m2$ (point group D_{3h}), with the needle direction coinciding with the c axis [Figs. 1(a)–1(c)]. Magnetic susceptibility measurements indicate that T_c is 6.1 K [Fig. 1(d)]. The samples were prepared and cleaved in Ar or N_2 atmosphere and moved into vacuum conditions without any exposure to air. The freshly cleaved single crystals have been measured in a backscattering geometry from the ac and bc surfaces [Figs. 1(b) and 1(c)]. We used the 488 and 514 nm lines of an Ar-Kr ion laser to focus a spot smaller than 5×5 μm^2 by using a microscope with a total incident power of less than 0.25 mW. The estimated laser heating is 6 K. The Raman scattering signal was analyzed by a Horiba Jobin Yvon T64000 spectrometer and collected by a liquid N_2 cooled CCD detector. The data were corrected for the CCD dark current and the luminescence background determined by extrapolating the featureless linear spectra between 400 and 750 cm^{-1}. The temperature-dependent measurements from 12 to 300 K were performed in a Janis liquid helium flow cryostat in a working vacuum of better than 2×10^{-6} mbar. The Raman spectra were obtained in all informative backscattering configurations, which correspond to $e^i e^s = XX$, ZZ, and XZ. Here, e^i and e^s are the polarizations of the incident and scattered light defined in the laboratory coordinates, with X and Z corresponding to the crystallographic axes a and c, respectively, and Y oriented at 30° from the b axis [Fig. 1(c)].

We also performed first-principles calculations using the projector augmented wave (PAW) method encoded in the Vienna *ab initio* simulation package (VASP) [12–14] and the generalized-gradient approximation (GGA) [15] for the exchange correlation functions. The cutoff energy was set to be 500 eV and the number of k points was set to $2 \times 2 \times 5$ for a $2 \times 2 \times 2$ supercell. The real-space force constants

*wlzhang@iphy.ac.cn
†p.richard@iphy.ac.cn

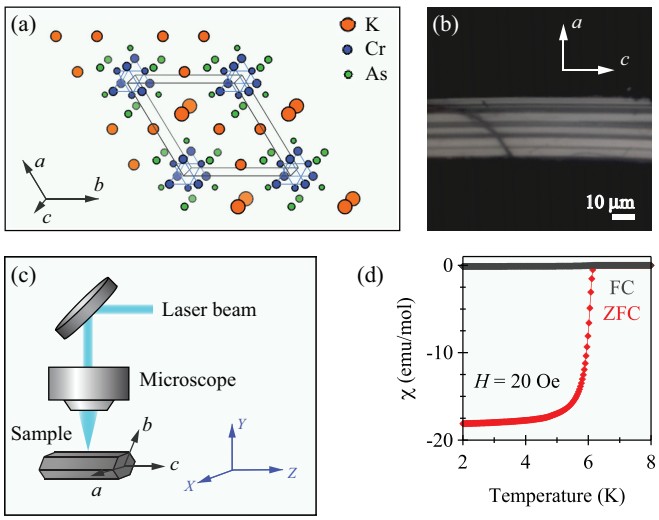

FIG. 1. (Color online) (a) Unit cell of $K_2Cr_3As_3$. The atoms from different layers are represented with different sizes. (b) Microscope photograph of the ac surface of a measured $K_2Cr_3As_3$ sample. (c) Optical setup and choice of crystallographic and laboratory coordinates. (d) Magnetic susceptibility of one sample from the same batch.

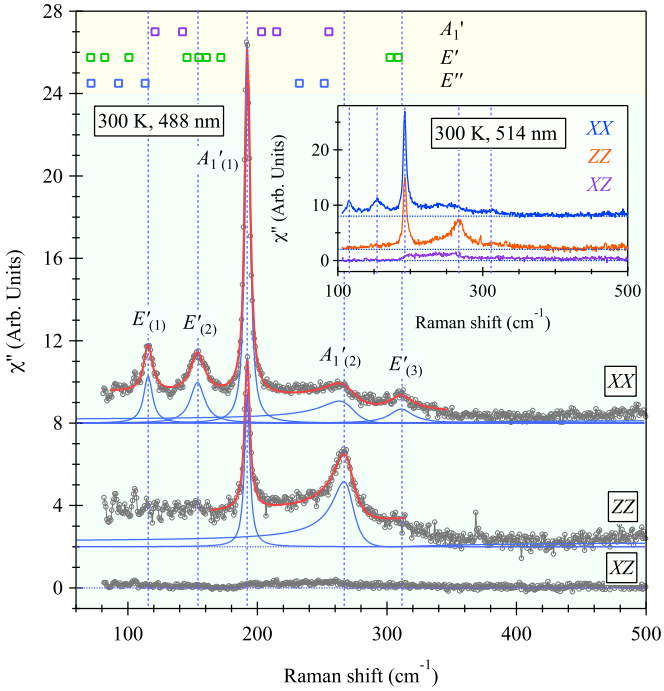

FIG. 2. (Color online) Raman susceptibility at 300 K measured under different polarization configurations with 488 nm laser excitation. Each peak can be fitted by a Lorentz or a Fano function for the spectra under XX and ZZ polarizations. The individual peak functions are represented by blue curves while the red curves represent the resulting fitted spectra. The squares at the panel top represent the calculated BZ center phonon energies (see Table I). From top to bottom are the calculated results for the A', E', and E'' modes, respectively. Inset: Raman susceptibility at 300 K under different polarizations with 514 nm laser excitation.

of the supercells were calculated in the density-functional perturbation theory (DFPT) [16] and the phonon frequencies were calculated from the force constants using the PHONOPY code [17]. As the Cr-Cr bond lengths are underestimated after relaxation of the lattice [10], which may be related to the strong spin fluctuations in this material, all phonon modes were calculated using the experimental lattice parameters [2].

With two formulas in one unit cell (i.e., 16 atoms), $K_2Cr_3As_3$ is characterized by 48 phonon vibrational modes at the Brillouin zone (BZ) center (Γ point). A group theory analysis shows that the corresponding irreducible representations defining the symmetry of the vibration modes are $[A_2'' + E'] + [5A_1' + 10E' + 5E''] + [5A_2' + 5A_2'']$, where the first, second, and third terms are the acoustic, Raman-active, and infrared-active modes, respectively. The corresponding Raman tensors R_i in the laboratory coordinates, which determine the intensity I of the Raman phonons according to $I = (e^s)^T R_i e^i$, are [18]

$$R_{A_1'} = \begin{pmatrix} a & 0 & 0 \\ 0 & a & 0 \\ 0 & 0 & b \end{pmatrix},$$

$$\left\{ R_{E_X'} = \begin{pmatrix} d & 0 & 0 \\ 0 & -d & 0 \\ 0 & 0 & 0 \end{pmatrix}, R_{E_Y'} = \begin{pmatrix} 0 & -d & 0 \\ -d & 0 & 0 \\ 0 & 0 & 0 \end{pmatrix} \right\},$$

$$\left\{ R_{E_X''} = \begin{pmatrix} 0 & 0 & c \\ 0 & 0 & 0 \\ c & 0 & 0 \end{pmatrix}, R_{E_Y''} = \begin{pmatrix} 0 & 0 & 0 \\ 0 & 0 & -c \\ 0 & -c & 0 \end{pmatrix} \right\}.$$

Here, a, b, c, and d refer to Raman tensor elements (not to be confused with the crystallographic directions). The XX polarization can couple to A_1' and E' modes, whereas the ZZ and XZ polarizations only couple to A_1' and E'' modes, respectively.

The Raman response in the XX, ZZ, and XZ polarization configurations recorded at room temperature under 488 nm laser excitation are plotted in Fig. 2. Similar results are obtained using the 514 nm laser excitation, as shown in the inset of Fig. 2. In the XX polarization we identify five Raman-active modes at 115.7, 154.1, 192.1, 267.0, and 311.0 cm^{-1}. In order to separate the phonon modes with A_1' and E' symmetries, we also recorded a spectrum in the ZZ polarization. In the ZZ polarization, the 192.1 and the 267.0 cm^{-1} peaks remain while the other three disappear. We thus conclude that the 192.1 cm^{-1} ($A'_{1(1)}$) and the 267.0 cm^{-1} ($A'_{1(2)}$) peaks have A_1' symmetry whereas the 115.7 cm^{-1} ($E'_{(1)}$), 192.1 cm^{-1}($E'_{(2)}$) and 311.0 cm^{-1}($E'_{(3)}$) peaks are characterized by E' symmetry. We also notice that the amplitude of $A'_{1(2)}$ increases in the ZZ polarization as compared to the XX polarization, in contrast to the amplitude of the $A'_{1(1)}$ mode which decreases in the XX polarized spectrum. This is due to the strong one-dimensional (1D) character of $K_2Cr_3As_3$, which leads to a strong anisotropy of the a and b terms in the Raman tensor. Despite their Raman activity under XZ polarization, no E'' symmetry mode is observed.

Although the symmetries of the Raman modes observed can be identified experimentally with certainty, their assignments to precise vibrational modes is not always unique as some discrepancies are observed between the experimental phonon

TABLE I. Raman-active phonon energy at Γ by calculation and experiment at 300 K and the atoms primarily involved. The subscript numbers of atoms refer to the two equivalent layers, as shown in Fig. 3(i).

No.	Symmetry	Calc. (cm^{-1})	Expt. (cm^{-1})	Main atoms involved
1	E'	30.648		Cr_1, Cr_2
2	E'	71.304		K_1, Cr_2, As_1
3	E''	71.528		K_1
4	E'	82.203		K_1, K_2, Cr_1, As_2
5	E''	92.773		K_1, Cr_2, As_2
6	E'	100.731	115.7	K_1, K_2
7	E''	113.377		K_1, Cr_1, As_1
8	A'_1	120.945		K_1
9	A'_1	142.218		K_1, Cr_1, Cr_2
10	E'	145.631		K_1, K_2, As_1
11	E'	154.749	154.1	K_1, Cr_2, As_1
12	E'	160.606		As_1, As_2
13	E'	171.732		K_1, Cr_1, Cr_2
14	A'_1	203.121	192.1	As_1, As_2
15	A'_1	214.914		Cr_1, Cr_2, As_1, As_2
16	E''	232.367		Cr_2
17	E''	251.674		Cr_1
18	A'_1	255.194	267.0	Cr_1, Cr_2
19	E'	302.336		Cr_1, As_2
20	E'	308.602	311.0	Cr_2, As_1

energies and the calculated values at the Γ point, which are given in Table I. The calculated energies are also indicated by the squares at the top of Fig. 2. By taking into account the peak symmetries and their proximity in energy with the calculated values, we tentatively assign $E'_{(1)}$, $E'_{(2)}$, and $E'_{(3)}$ to phonons No. 6, No. 11, and No. 20, respectively, while we assign $A'_{1(1)}$ and $A'_{1(2)}$ to phonons No. 14 and No. 18, respectively. As we will discuss below, one possible candidate to explain the discrepancies between experiments and calculations is the presence of a magnetoelastic coupling, which is neglected in the calculations.

In contrast to all the other peaks observed, the $A'_{1(2)}$ feature has a quite asymmetric line shape. In Fig. 2 we show that the Raman response in the XX and ZZ polarization configurations can be fitted by the equation

$$\chi''(\omega) = \Sigma_i T_i L(\omega,\omega_i,\Gamma_i) + T_F F(\omega,\omega_F,\Gamma_F,q), \qquad (1)$$

where $L(\omega,\omega_i,\Gamma_i) = \frac{\Gamma_i}{(\omega-\omega_i)^2+\Gamma_i^2}$ is the Lorentz function characteristic of the normal phonon modes and $F(\omega,\omega_F,\Gamma_F,q) = \frac{1}{\Gamma_F q^2}\frac{[q+\alpha(\omega))]^2}{[1+\alpha(\omega)^2]}$ with $\alpha(\omega) = \frac{\omega-\omega_F}{\Gamma_F}$ is the Fano function [1], well suited for the asymmetric peak at 267 cm^{-1} ($A'_{1(2)}$). Here, T_i (T_F) is the amplitude of the ith phonon mode, while ω_i (ω_F) and Γ_i (Γ_F) are the bare phonon energy and linewidth, respectively. The $1/q$ value is commonly used in Raman spectroscopy as a measure of the electron-phonon coupling strength [19], such as in the cuprates [20,21], Fe-based superconductors [21,22], and Bi-based superconductors [23]. However, a careful interpretation would necessitate considerations on electron-phonon matrix vertex elements and the electronic structure as well. For $K_2Cr_3As_3$ we get $1/q = -0.29 \pm 0.03$ from the spectrum of ZZ polarization at 300 K. The electron-phonon coupling strength can also be estimated from the phonon linewidth of the phonon modes for all $\mathbf{q}$ vectors by using the Allen's formula [24,25],

$$\lambda_i = \frac{2\gamma_i}{\pi N(E_F)\omega_{bi}^2}. \qquad (2)$$

Raman scattering only allows for $\mathbf{q} = \mathbf{0}$ excitations. As an approximation of the integrations of all $\mathbf{q}$, we estimate the strength $\lambda_F = 0.054$ using $\omega_{bi} = 267.0$ cm^{-1} as the $A'_{1(2)}$ phonon bare frequency at 12 K, $\gamma_i = 13.5$ cm^{-1} as the $A'_{1(2)}$ phonon linewidth, and $N(E_F) = 18$ eV^{-1} as the electron density of states per unit cell at the Fermi level [7]. Although measurements below T_c and a complete knowledge of all the phonon modes at all $\mathbf{q}$, as well as of the experimental electronic structure, would be necessary to make a conclusive statement, the contribution of the $A'_{1(2)}$ mode to $\lambda = 0.054$ seems too small to afford for the T_c of this material within the BCS picture [26,27] using our simple approximations.

We show in Figs. 3(a) and 3(b) the temperature evolution from 12 to 300 K of the intensity plot of the phonon spectra obtained with 488 nm laser excitation in the XX and ZZ polarization configurations. The spectra at all temperatures are qualitatively similar to the data recorded at 300 K. The phonon energies ω_i and linewidths Γ_i obtained by fitting the data to Eq. (1) for $E'_{(1)}$, $E'_{(2)}$, and $A'_{1(1)}$ are plotted in Figs. 3(c)–3(f). We notice that $E'_{(1)}$ undergoes unconventional softening of the central energy and broadening of the linewidth upon cooling. For the low temperatures, the line shape has distortion from the Lorentz fit, which may imply that there is more than one phonon mode close to this energy [Fig. 3(k)], however, due to the limitation of the instrumental resolution and phonon linewidth, we are not able to distinguish them. The Raman response function of the unusual $A'_{1(2)}$ phonon under YY polarization and the fitting curve at representative temperatures are shown in Fig. 3(g). A distorted line shape is observed at all temperatures. Indeed, Fig. 3(h) shows that the coupling constant $1/q$ extracted from the fits varies only a little with temperature.

Although we cannot exclude that the Fano line shape of the $A'_{1(2)}$ phonon is purely due to the electron-phonon coupling, many indications suggest that a coupling between the lattice and magnetic fluctuations is involved. As mentioned above, the experimental phonon energies are particularly difficult to reproduce from the calculations, possibly due to the influence of magnetic fluctuations. Additional information can be deduced from the spectral line shape of the various Raman peaks. In Figs. 3(i) and 3(j), we illustrate the vibration configuration of the sharp and symmetric $A'_{1(1)}$ phonon peak and that of the broader and asymmetric $A'_{1(2)}$ phonon mode, respectively. Unlike the $A'_{1(1)}$ mode that mainly involves in-phase coplanar vibrations of the As atoms, the $A'_{1(2)}$ mode involves mainly the in-phase coplanar vibrations of the Cr atoms. Consequently, the latter vibration mode has a much stronger impact on the intralayer Cr-Cr bonding. Interestingly, a recent theoretical study indicates that the next-neighbor Cr-Cr exchange interaction is by far the strongest in this system [10], and the modulation of the Cr-Cr intralayer distance should thus lead to the strongest magnetoelastic

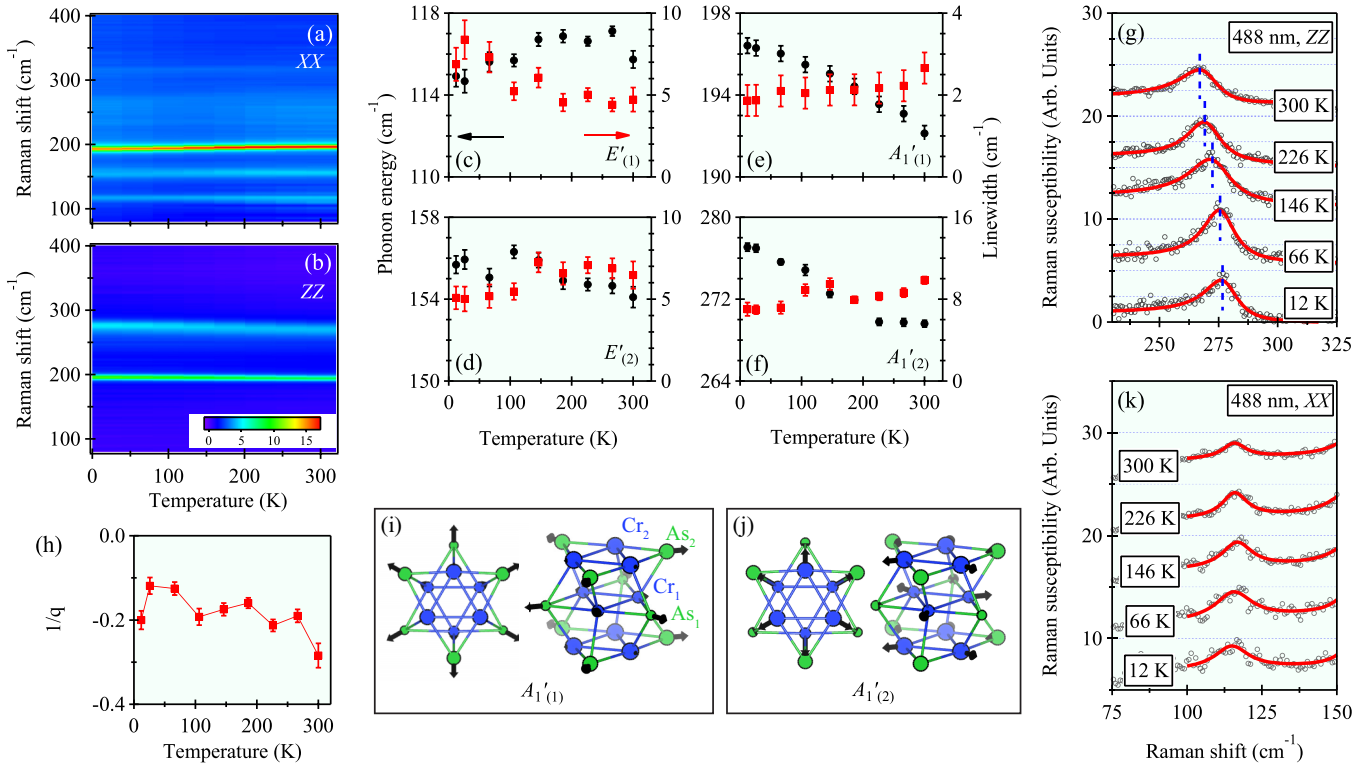

FIG. 3. (Color online) (a), (b) Intensity plot of the temperature dependence of the Raman susceptibility under XX and ZZ polarizations, respectively. (c)–(f) Temperature evolution of the phonon energies and the linewidths of the $E'_{(1)}$, $E'_{(2)}$, $A'_{1(1)}$, and $A'_{1(2)}$ peaks from the fitting of the data in (a) and (b) by Eq. (1). (i), (j) Atomic displacements in the CrAs tube of the $A'_{1(1)}$ and $A'_{1(2)}$ modes, respectively, from the top view and side view. (g), (k) Zoom of the Raman response function and the Fano (Lorentz) fitting curve of the $A'_{1(2)}$ ($E'_{(1)}$) phonon peak at representative temperatures. (h) Temperature dependence of the electron-phonon coupling strength $1/q$ by fitting data in (b) by Eq. (1).

effect. The importance of the intralayer Cr-Cr distance is also supported by the sensitivity of superconductivity to isovalent substitution of K with larger Cs [3] or Rb [4] atoms, and to applying hydrostatic or uniaxial pressure [28]. Even though our results do not allow us to comment directly on the unconventional nature of superconductivity in $K_2Cr_3As_3$, they certainly suggest that the magnetic fluctuations reported in this system are coupled to the electronic structure via lattice vibrations, which may be of crucial importance in elaborating models for superconductivity in this material.

We acknowledge P. Zhang, X.-X. Wu, S.-F. Wu, and D. Chen for discussions. This work was supported by grants from MOST (No. 2010CB923000, No. 2011CBA001000, No. 2011CBA00102, No. 2012CB821403, and No. 2013CB921703) and NSFC (No. 11004232, No. 11034011/A0402, No. 11234014, No. 11274362, and No. 11474330) of China, and by the Strategic Priority Research Program (B) of the Chinese Academy of Sciences, Grant No. XDB07020100.

W.-L.Z. and H.L. contributed equally to this work.

[1] U. Fano, Phys. Rev. **124**, 1866 (1961).
[2] J.-K. Bao, J.-Y. Liu, C.-W. Ma, Z.-H. Meng, Z.-T. Tang, Y.-L. Sun, H.-F. Zhai, H. Jiang, H. Bai, C.-M. Feng, Z.-A. Xu, and G.-H. Cao, Phys. Rev. X **5**, 011013 (2015).
[3] Z.-T. Tang, J.-K. Bao, Z. Wang, H. Bai, H. Jiang, Y. Liu, H.-F. Zhai, C.-M. Feng, Z.-A. Xu, and G.-H. Cao, Sci. China Mater. **58**, 16 (2015).
[4] Z.-T. Tang, J.-K. Bao, Y. Liu, Y.-L. Sun, A. Ablimit, H.-F. Zhai, H. Jiang, C.-M. Feng, Z.-A. Xu, and G.-H. Cao, Phys. Rev. B **91**, 020506 (2015).
[5] H. Z. Zhi, T. Imai, F. L. Ning, J.-K. Bao, and G.-H. Cao, Phys. Rev. Lett. **114**, 147004 (2015).
[6] G. M. Pang, M. Smidman, W. B. Jiang, J. K. Bao, Z. F. Weng, Y. F. Wang, L. Jiao, J. L. Zhang, G. H. Cao, and H. Q. Yuan, Phys. Rev. B **91**, 220502 (2015).
[7] X. Wu, F. Yang, C. Le, H. Fan, and J. Hu, arXiv:1503.06707.
[8] W. Wu, J. Cheng, K. Matsubayashi, P. Kong, F. Lin, C. Jin, N. Wang, Y. Uwatoko, and J. Luo, Nat. Commun. **5**, 5508 (2014).
[9] H. Jiang, G. Cao, and C. Cao, arXiv:1412.1309.
[10] X.-X. Wu, C.-C. Le, J. Yuan, H. Fan, and J.-P. Hu, Chin. Phys. Lett. **32**, 57401 (2015).
[11] T. Kong, S. L. Bud'ko, and P. C. Canfield, Phys. Rev. B **91**, 020507 (2015).
[12] G. Kresse and J. Hafner, Phys. Rev. B **47**, 558 (1993).
[13] G. Kresse and J. Furthmüller, Comput. Mater. Sci. **6**, 15 (1996).
[14] G. Kresse and J. Furthmüller, Phys. Rev. B **54**, 11169 (1996).

[15] J. P. Perdew, K. Burke, and M. Ernzerhof, Phys. Rev. Lett. **77**, 3865 (1996).
[16] S. Baroni, P. Giannozzi, and A. Testa, Phys. Rev. Lett. **58**, 1861 (1987).
[17] A. Togo, F. Oba, and I. Tanaka, Phys. Rev. B **78**, 134106 (2008).
[18] E. Kroumova, M. Aroyo, J. Perez-Mato, A. Kirov, C. Capillas, S. Ivantchev, and H. Wondratschek, Phase Transitions **76**, 155 (2003).
[19] M. Klein, *Electronic Raman Scattering, Light Scattering in Solids I* (Springer, Berlin, 1975).
[20] S. L. Cooper, M. V. Klein, B. G. Pazol, J. P. Rice, and D. M. Ginsberg, Phys. Rev. B **37**, 5920 (1988).
[21] A.-M. Zhang and Q.-M. Zhang, Chin. Phys. B **22**, 87103 (2013).
[22] L. Chauvière, Y. Gallais, M. Cazayous, M. A. Méasson, A. Sacuto, D. Colson, and A. Forget, Phys. Rev. B **84**, 104508 (2011).
[23] S. F. Wu, P. Richard, X. B. Wang, C. S. Lian, S. M. Nie, J. T. Wang, N. L. Wang, and H. Ding, Phys. Rev. B **90**, 054519 (2014).
[24] P. B. Allen, Phys. Rev. B **6**, 2577 (1972).
[25] P. B. Allen, Solid State Commun. **14**, 937 (1974).
[26] W. L. McMillan, Phys. Rev. **167**, 331 (1968).
[27] R. Dynes, Solid State Commun. **10**, 615 (1972).
[28] Z. Wang, V. Sidorov, Q. Wu, J. Bao, Z. Tang, W. Yi, J. Guo, Y. Zhou, S. Zhang, C. Zhang, G. Cao, L. Sun, and Z. Zhao, arXiv:1502.04304.